Onset of irreversibility and chaos in amorphous solids under periodic shear

Ido Regev, Turab Lookman, and Charles Reichhardt
Center for Nonlinear Studies and Theoretical Division, Los Alamos National Laboratory, Los Alamos, New Mexico 87545, USA
(Received 11 March 2013; revised manuscript received 21 October 2013; published 2 December 2013)

A fundamental problem in the physics of amorphous materials is understanding the transition from reversible to irreversible plastic behavior and its connection to yield. Currently, continuum material modeling relies on phenomenological yield thresholds, however in many cases the transition from elastic to plastic behavior is gradual, which makes it difficult to identify an exact yield criterion. Here we show that under periodic shear, amorphous solids undergo a transition from repetitive, predictable behavior to chaotic, irregular behavior as a function of the strain amplitude. In both the periodic and chaotic regimes, localized particle rearrangements are observed. We associate the point of transition from repetitive to chaotic behavior with the yield strain and suggest that at least for oscillatory shear, yield in amorphous solids is a result of a "transition to chaos."

DOI: 10.1103/PhysRevE.88.062401 PACS number(s): 62.20.F−, 05.20.−y, 83.60.La, 83.60.Wc

I. INTRODUCTION

Amorphous solids such as plastics, window glass, and amorphous metals are an important and ubiquitous form of matter. Industrial processing of such materials commonly involves plastic deformation. Although a microscopic mechanism of plastic deformation in these materials was identified [1–3], the collective behavior on the mesoscale is still being debated. Our current theoretical understanding of amorphous solids includes mainly mean-field statistical mechanics theories that are based on the assumption that the microscopic dynamics of plasticity is stochastic. Therefore, it is described in terms of probability distributions which model the evolution of localized particle rearrangements exhibiting a transition from jammed to flowing behavior [4–7]. Recent experiments and simulations on superconductor vortices, dilute colloidal dispersions, and loosely packed granular materials showed that these materials undergo a transition from reversible to irreversible diffusive behavior by varying the strength of an oscillatory external field [8–17]. In this work, we study highly condensed amorphous solids (well above the jamming transition) under oscillatory shear and show that for small strain amplitudes, these systems evolve into periodic limit cycles during which particles change their positions but follow the same trajectories for consecutive cycles. These rearrangements are dissipative and thus result in energy fluctuations, but for small strains they are completely repetitive. Therefore, the work being done on the material is transformed wholly into heat, and structural rearrangements are reversible. Above a critical strain amplitude, the system does not settle into a limit cycle and the motion is chaotic with a positive maximal Lyapunov exponent. This allows us to define a yield point with a physical meaning. A yield point can be difficult to determine from a standard stress-strain curve since the behavior can be monotonic and there need not be a stress peak, as this depends on the way that the system is prepared. For example, the solid green curve in Fig. 1 was prepared by a fast quench compared to the dashed blue curve in the inset, which was prepared via a slow quench. Identifying and understanding the underlying dynamical behavior opens the possibility for a quantitative description of the structural changes occurring in these systems after yield and their relation to the dynamics.

The paper is organized as follows. In Sec. II we describe the system and simulations methodology. In Sec. III we describe the main finding of this paper, i.e., the characterization of a dynamical transition and its identification as a "transition to chaos." Section IV describes the dynamics in the periodic regime, and finally we summarize the results in Sec. V.

II. SIMULATIONS

We perform molecular-dynamics simulations of a system of N-point particles in two and three dimensions interacting via a pairwise potential where the effective radius of half the particles is 1.4 times larger than the other half. We use the mass m of the particles, the typical interaction distance σ, and the typical interaction energy ϵ (see Appendix A for details on the potential and on the simulations performed in three dimensions) to define reduced units for the energy ($E \to E/\epsilon$), the stress $\sigma_{xy} \to \sigma_{xy}/(\epsilon/\sigma^3)$, the number density $\rho \to \rho/(1/\sigma^3)$, and the time $t \to t/(\epsilon/m\sigma^2)^{1/2}$. Positions of particles are given in terms of $q \to q/L$, where L is the system size. The sample is kept at a constant number density $\rho = 0.75$ in the reduced units, which is significantly higher than the jamming transition. Amorphous solids are prepared by equilibrating systems of particles at a high temperature and than quenching them to zero temperature using a minimization algorithm [18]. The material is subject to small steps of shear ($\Delta\gamma = 10^{-4}$) using the Lees-Edwards boundary conditions. The dynamics under shear is quasistatic (after each shearing step the energy was minimized using the FIRE minimization algorithm [18]) or, in one case, overdamped Brownian motion with zero or small temperature (at zero temperature, the quasistatic and overdamped dynamics give the same qualitative behavior). The strain is applied in a periodic manner: First, positive strain steps are applied. When a maximal predecided strain $\epsilon_{\max}$ is reached, the strain is reversed by applying strain steps in the opposite direction. This proceeds until the strain reaches the negative value of the maximal strain $-\epsilon_{\max}$. At this point the strain steps are reversed until the system returns to zero strain, completing the cycle. The cycle is then repeated.

III. TRANSITION TO CHAOS

For small strain amplitudes, we observe that after a number of cycles the response of the material becomes completely

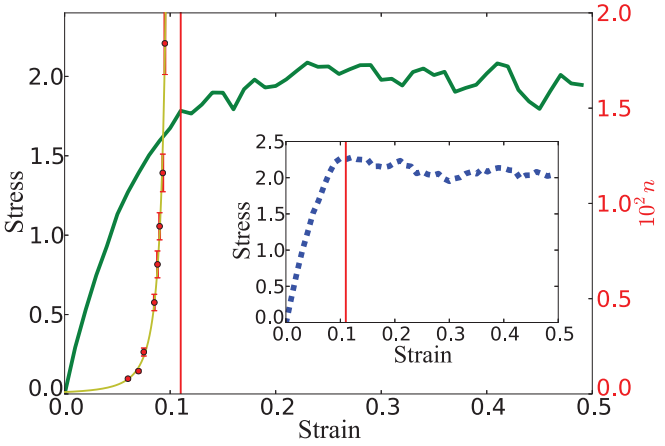

FIG. 1. (Color online) Stress-strain curve from molecular-dynamics simulations for 16 384 particles under quasistatic shear. Red dots represent the number of cycles, n, required to reach periodic behavior under oscillatory shear (the scale is on the right side of the figure in red). The vertical red line is the strain amplitude for which the time to reach reversible behavior diverges. Inset: stress-strain behavior for the same parameters as the solid green curve but with different initial particle configurations—the vertical red line is the same as in the main figure.

repetitive (see Fig. 2). However, the response is not immediately reversible and there is a transient nonperiodic behavior before the system reaches a stable limit cycle. The transient times increases with the strain amplitude until it is so large that the system does not reach a limit cycle. This behavior is similar to that observed in the shearing of colloidal dispersions [10]. To measure the time it takes for the system to reach a periodic limit cycle, we define a cycle decorrelation function for the potential energy $U(t)$:

$$R(n) = \int dt |U(t,n) - U(t,n-p)|. \quad (1)$$

When $p = 1$, this function compares the difference between potential energy fluctuations in two consecutive cycles (n is the number of cycles that the system underwent). For small strain amplitudes, this function will reach a value close to zero after n cycles. However, in some cases the system reaches a limit cycle

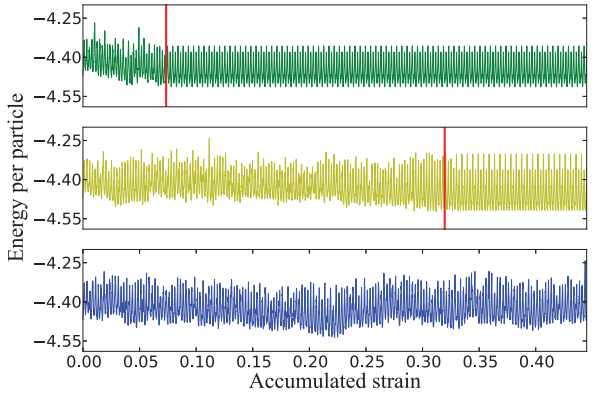

FIG. 2. (Color online) Transient behavior of the potential energy before reaching a limit cycle for three different strain amplitudes (strain amplitude growing from top to bottom). Vertical red lines are the points at which periodic behavior begins.

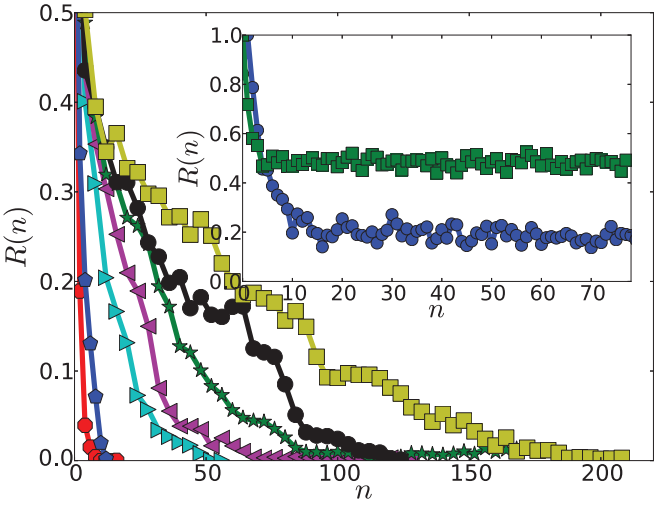

FIG. 3. (Color online) Cycle decorrelation function as a function of the number of cycles, for system size $N = 16\,384$ particles for strain amplitudes $\gamma = 0.06$, 0.07, 0.75, 0.85, 0.88, 0.09, 0.093, and 0.095 (from left to right). Inset: The same function for strain amplitudes $\gamma = 0.12$ (blue circles) and $\gamma = 0.15$ (green rectangles).

of periodicity p larger than 1. Therefore, if periodic behavior is not observed, we increase p by 1 and recalculate the function. We repeat this process until we find a value of p for which the function reaches $R(n) = 0$ for some n. If periodicity smaller than $p = 11$ is not observed, we set p to its default value $p = 1$. In all cases, periodicity larger than $p = 5$ was not observed. In Fig. 3 we show this function averaged over 30 different samples of size $N = 16\,384$, each prepared from a different initial condition in the liquid state and then quenched using the same protocol that was used to create the solid green curve in Fig. 1. One can observe that for the strain amplitudes $\gamma = 0.06$, 0.07, 0.75, 0.85, 0.88, 0.09, 0.093, and 0.095, the function relaxes, after a transient time, to zero, while for larger strain amplitudes ($\gamma = 0.12, 0.15$) the function $R(n)$ does not decay to zero but relaxes to some asymptotic finite value (we verified separately that for single systems sheared at strain amplitudes $\gamma = 0.12, 0.15$, the system does not become periodic even for $n > 1000$ cycles). In Fig. 4 we show that the relaxation time, the time it takes the cycle-decorrelation function to reach below 1% of its initial value, follows a power law with a critical point at $\gamma_c = 0.11$. This critical strain amplitude is close to the yield strain as estimated from the dashed blue linear stress-strain curve in the inset of Fig. 1, even though for the oscillatory shear we have used the faster quench protocol that corresponds to the solid green curve in Fig. 1. From this power-law behavior it is clear that the system undergoes a dynamical transition. However, a question that arises is what kind of transition are we observing and is there a fundamental difference in the dynamics of the system before and after the transition. The fact that we observe a transition from a repetitive to random behavior in a deterministic, dissipative system (no external noise is added) suggests a "transition to chaos." This is a well-known phenomenon observed in various dynamical systems, from the low-dimensional Lorenz system [19] to high-dimensional coupled chaotic maps [20], and it involves a divergence (usually power-law) in the time it takes the system to reach periodic behavior as a parameter is varied. For certain

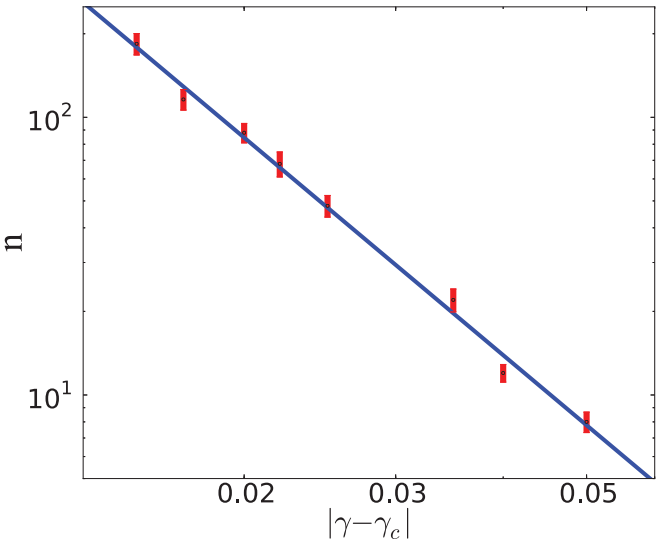

FIG. 4. (Color online) Slowing down: Log-log plot of the typical number of cycles n before reaching periodic behavior (including error bars) as a function of the strain amplitude γ.

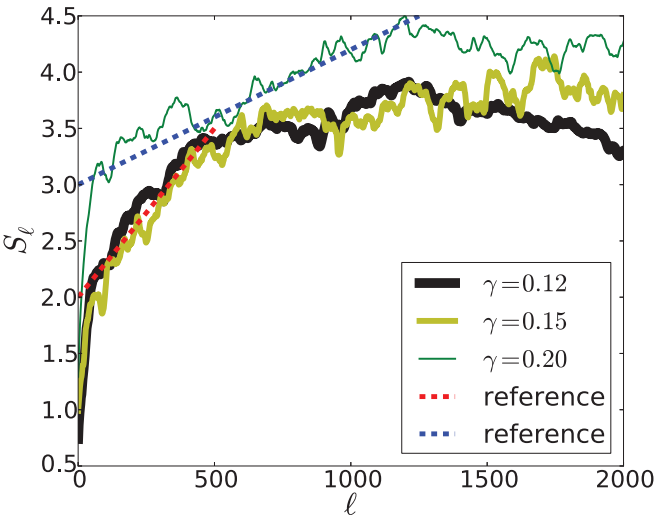

FIG. 5. (Color online) Estimation of maximal Lyapunov exponents: The function S_ℓ of the time delay ℓ for a system of size $N = 4096$ under oscillatory shear in different strain amplitudes larger than the critical amplitude. The dashed straight lines are shown as a guide to the eye.

control parameters, the dynamics is chaotic and never repeats itself.

The main indication that a system exhibits chaotic behavior is sensitivity to initial conditions: trajectories starting from close-by initial conditions diverge exponentially [21,22]. The sensitivity to initial conditions is estimated by measuring the maximal Lyapunov exponent λ which describes the rate of growth of the distance between two phase-space trajectories (solutions of the equations of motion with different initial conditions) $\mathbf{x}(t)$ and $\mathbf{x}_\epsilon(t)$, which are initially separated by a diminishing distance $|\mathbf{x}(0) - \mathbf{x}_\epsilon(0)| = \epsilon$:

$$\lambda_{\max} = \lim_{t\to\infty}\lim_{\epsilon\to 0}\frac{1}{t}\ln\frac{|\mathbf{x}(t)-\mathbf{x}_\epsilon(t)|}{\epsilon}. \qquad (2)$$

For a periodic system $\lambda_{\max} = 0$, whereas a chaotic system will have $\lambda_{\max} > 0$. We calculate the maximal Lyapunov exponent by analyzing the discrete time series of the potential energy $u_i = \{u_0, u_1, u_2, \ldots\}$ using the method described in Kantz *et al.* [22,23]. The algorithm produces a function S_ℓ of the time delay ℓ:

$$S_\ell = \frac{1}{|\mathcal{W}|}\sum_i \ln\left(\frac{1}{|\mathcal{U}_i|}\sum_k \frac{|u_{i+\ell}-u_{k+\ell}|}{\epsilon}\right), \qquad (3)$$

where $|\mathcal{U}_i|$ is the total number of points which are initially ϵ close to point u_i and $|\mathcal{W}|$ is the total number of initial point u_i chosen by the algorithm. The function S_ℓ measures the logarithm of the average rate of separation of near-by phase-space trajectories (see Appendix B for an extended discussion). This function shows a distinct behavior when calculated for chaotic time series: for an intermediate range of ℓ, it will have a linear, positive slope where the value of the slope is the value of the Lyapunov exponent. In Fig. 5, we plot the function S_ℓ for a time series of potential energy values for a system of size $N = 4096$ sheared at maximal strain amplitudes $\gamma = 0.12$, 0.15, and 0.2 all above the critical amplitude. In all three cases, the function exhibits linear behavior for intermediate values of ℓ indicating a positive Lyapunov exponent and hence chaotic behavior. These results are consistent with previous results for the maximal Lyapunov exponent for amorphous solids under *linear* shearing obtained in experiments [24] and simulations [25]. For the technical details on the derivation of the function S_ℓ, its relation to the maximal Lyapunov exponent $\lambda_{\max}$, and the parameters used, see Appendix B. These results suggest that amorphous solids undergo a transition to chaos at a strain amplitude coincident with yield at least under oscillatory shear. One should note that a transition to chaos is quite distinct from a nonequilibrium phase transition, and although it shows behavior similar to critical slowing down, it is not necessarily accompanied by critical fluctuations and a growing correlation length, which are expected in a nonequilibrium phase transition such as directed percolation. The critical slowing down exponent for this system was found to be $\nu \approx 2.6$, as compared to the value $\nu \approx 1.33$ observed by Corte *et al.* [10] in experiments and simulations of dispersed colloidal suspensions under oscillatory shear. This may not be too surprising as their experiments and accompanying simulations were performed in a dilute limit where particles interact mostly by direct collisions, whereas in our system long-range interactions mediated by the stress field are important. Even though both systems show a transition to irreversible behavior, the nature of the transition may be quite different. Our exponent is also different from $\nu \approx 3.33$ obtained for the well-studied transition to chaos in the Lorenz system [19]. However, since it is not clear if the transition to chaos forms universality classes, the values of ν are not necessarily a faithful indicator of different mechanisms for the transition.

IV. ANALYSIS OF PERIODIC BEHAVIOR

As we explained above, for strain amplitudes smaller than the critical value, after a transient regime, the system shows fluctuating but periodic behavior. This resembles the reversible regime of dilute colloidal systems, of the types

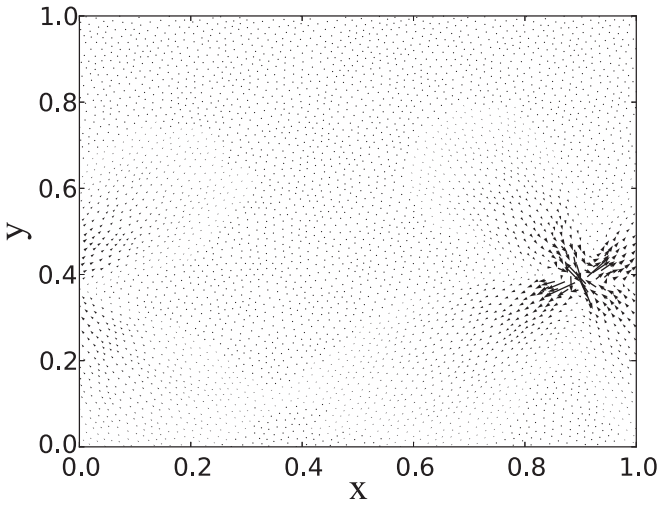

FIG. 6. Displacement field after a local particle rearrangement.

studied in [10,11]. However, in these systems, the dynamics is quite trivial since particles are no longer in contact. On the contrary, in the highly condensed state studied here, particles change positions and rearrange in a nontrivial manner, causing nonaffine deformation, even during a reversible limit cycle. Typically, this involves a large number of rearrangements of the T1 type (two next-nearest neighbors becoming nearest neighbors) which generate elastic-inclusion-like displacement fields (see Fig. 6) and appear as energy drops in the potential energy time series. In Fig. 7 we see three different limit cycles all simulated with the same system size and strain amplitude but with different initial conditions. We observe that whereas the period is the same, the details of the cycles (energy fluctuations) depend on the initial configuration. The repetitive behavior can also be observed by following the trajectory of any single particle over consecutive cycles (blue and yellow lines in Fig. 8). The nonaffine nature of the displacement of the particle is clear in the figure. One should note that contrary to the usual notion, the rearrangement events that we observe

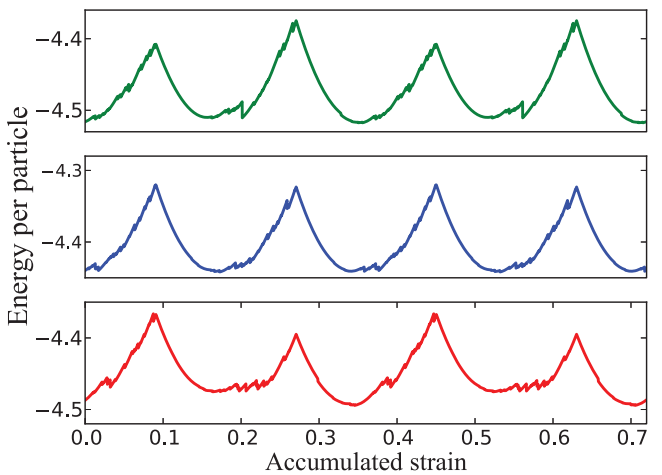

FIG. 7. (Color online) Several different limit cycles that were obtained using the same control parameters (number of particles, shearing steps, amplitude of shear) but different initial conditions.

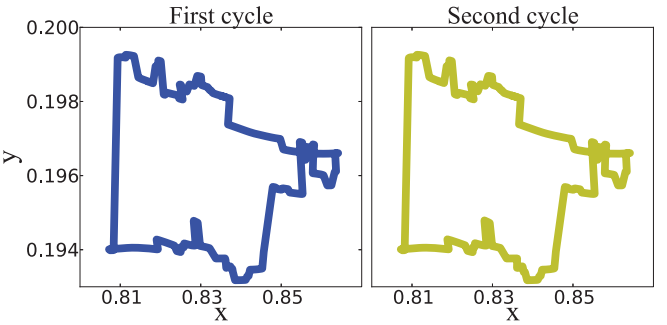

FIG. 8. (Color online) Two consecutive trajectories of one particle taken when the system is in a limit-cycle. The trajectories are very similar.

in the limit cycles are completely repetitive so that one can think of them as an extension of the notion of elasticity.

In Fig. 9, energy drops (rearrangement events) are identified and marked as black lines. The points in the limit cycle where these drops occur are marked as black dots in the columns of Fig. 10, where time advances from bottom to top. The x axis in Fig. 10 is the strain amplitude. This is repeated for different strain amplitudes with the same initial conditions. We observe that for small strain amplitudes, limit cycles that start from the same initial conditions are similar to each other, and an increase of the strain amplitude changes the limit cycle in a gradual manner. However, for large strain amplitudes, small increments in the strain amplitude result in a completely different limit cycle. We believe that this is a manifestation of the coexistence of many different limit cycles which occupy different parts of the state space and of the existence of "riddled basins of attraction" where infinitesimally close initial points in state space lead to completely different attractors [21,26]. In Fig. 11 we show the effect of applying Langevin noise to a system that is already in a limit cycle (these simulations were performed using overdamped dynamics). After a few cycles, the system escapes from the initial limit cycle and settles in a different limit cycle. This is another indication that there are a large number of nearby limit cycles, and it also shows that a limit cycle can exist with thermal fluctuations.

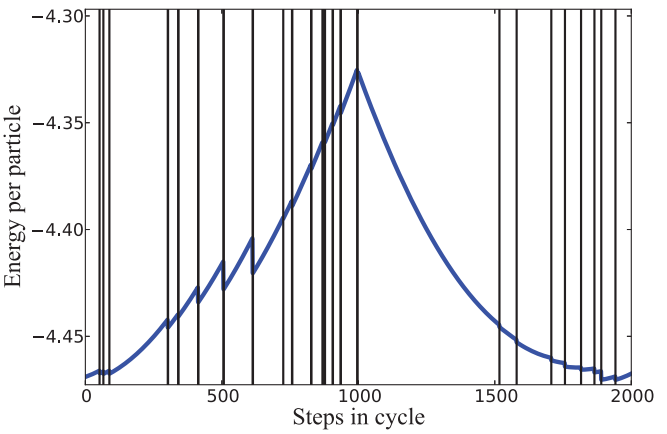

FIG. 9. (Color online) Analysis of one limit cycle with a certain strain amplitude: Energy drops (rearrangement events) are identified and marked as vertical black lines on this curve.

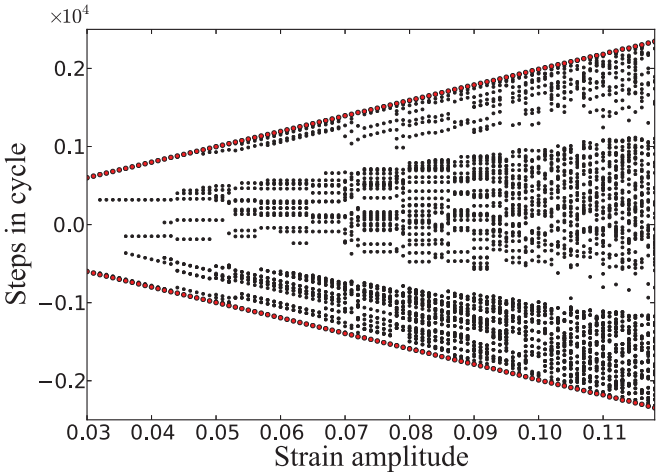

FIG. 10. (Color online) A plot of the position of energy drops (marked as black dots) on the limit cycle as a function of the strain amplitude (x axis) for one system of size $N = 1024$. The y axis is the time inside a limit cycle.

While the limit cycles that are shown in Fig. 7 repeat themselves after one cycle, for large strain amplitudes we observed cycles that repeat themselves after two, three, four, and five cycles (see Fig. 12), which is a phenomenon observed in many dynamical systems and in some cases can lead to a transition from periodic to chaotic behavior. This can happen in systems that show "frequency locking" or "period-doubling bifurcations." In a system showing a transition to chaos due to period doubling, the period of the limit cycle doubles for certain values of the control parameters. A succession of period doubling bifurcations (a period doubling cascade) leads to an infinite period and chaos. It is still too early to judge whether this behavior is the cause of the transition to chaos in this system.

The emergence of chaotic behavior can explain an important aspect of amorphous solids. In previous studies [27–29]

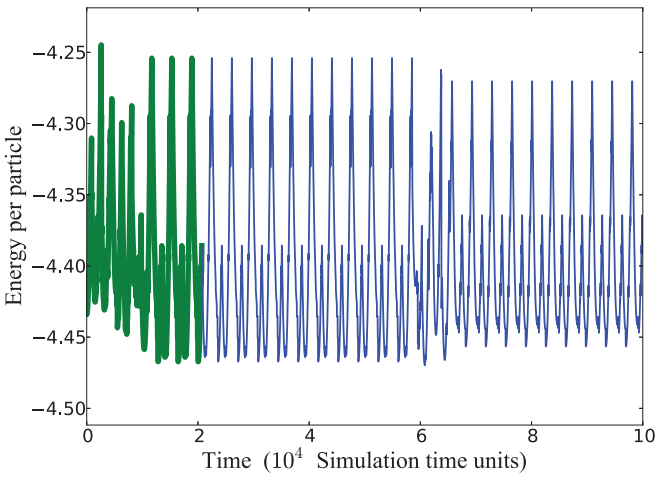

FIG. 11. (Color online) Effect of thermal noise: The system relaxes into a limit cycle after initial overdamped dynamics (green thick line). It is then subject to the same dynamics accompanied by a small Langevin noise. After some time it "hops" to another limit cycle.

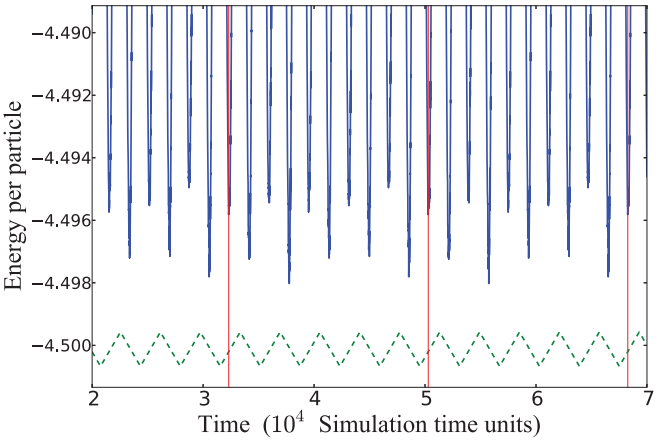

FIG. 12. (Color online) Periodic limit cycles with period 5 at strain amplitude $\gamma = 0.09$. The dashed green line is the applied strain (not to scale). Vertical red lines represent the start and the end of a cycle.

it was shown that the effective or "fictive" temperature that describes the structure of an amorphous solid depends on the initial quench of the system. However, when the material is deformed, the effective temperature of systems that were quenched using different cooling protocols converges to the same steady-state value which depends on the work performed on the system (and on the thermal bath temperature, when it is larger than zero). This has been described as overaging or rejuvenation of the amorphous solid [27], depending on whether the effective temperature increases or decreases. We can understand this behavior in terms of the onset of chaos. The existence of a positive maximal Lyapunov exponent is an indication that the system is not only chaotic, but that the dynamics is ergodic on a chaotic attractor which occupies part of the state space (this is different from ergodicity in Hamiltonian systems in which the entire state space for a given energy is explored). Since every initial condition ends up on the attractor, and the dynamics on the attractor is ergodic, averaged observables will eventually show the same values independent of the initial configuration.

V. CONCLUSIONS

In summary, we have examined the physics of yield in an amorphous solid under an oscillatory shear, and we showed that it is related to a transition to chaos. The behavior is similar to that observed in dilute colloidal suspensions and granular matter [10–13], even though our system is highly condensed. Further work is required to clarify the basis for the onset of chaos in this system. Our results may be corroborated by experiments on bulk metallic glasses as well as colloidal amorphous solids subject to slow oscillatory shear. Mean-field theories, such as the shear transformation zone theory [4], show a dynamical transition between jammed and flowing behavior, however we observe that the nature of fluctuations in the two regimes is fundamentally different, which cannot be captured in mean-field theories. The yield transition that we observe is currently attracting growing interest and is being studied in experiments on colloidal systems [17,30] and in

simulations of amorphous solids [31]. Here we propose a theoretical framework for the origin of this transition.

ACKNOWLEDGMENTS

We would like to thank Paul Chaikin, Colm Connaughton, Bob Ecke, Nicholas Ouellette, and Eran Bouchbinder for useful discussions. We would like to thank LANL institutional computing for resources. This work was carried out under the auspices of the U.S. Department of Energy at Los Alamos National Laboratory under Contract No. DE-AC52-06NA25396.

APPENDIX A: PAIRWISE POTENTIALS IN TWO AND THREE DIMENSIONS

For the two-dimensional system, we use the potential

$$U(r) = \begin{cases} \epsilon\left[\left(\frac{\sigma}{r}\right)^{12} - \left(\frac{\sigma}{r}\right)^{6} + \frac{1}{4} - h_0\right], & r \leqslant \sigma x_0, \\ \epsilon h_0 P\left(\frac{\frac{r}{\sigma} - x_0}{x_c}\right), & \sigma x_0 < r \leqslant \sigma(x_0 + x_c), \\ 0, & r > \sigma(x_0 + x_c), \end{cases} \tag{A1}$$

which was developed in [32] and consists of the repulsive part of the standard Lennard-Jones potential, connected via a hump to a region that is smoothed continuously to zero. The point x_0 is the position at which the LJ potential is minimal, $x_0 \equiv 2^{1/6}$, and the position where the potential vanishes is $\sigma(x_0 + x_c)$. The parameter h_0 determines the depth of the minimum. The polynomial $P(x)$ is chosen as

$$P(x) = \sum_{i=0}^{6} A_i x^i \ . \tag{A2}$$

with the coefficients given in Table I.

To supplement the simulations in two dimensions, we also run simulations of a binary mixture (1:1.4) of repulsive soft spheres using the potential $U(r) \propto \frac{1}{r^{12}}$ in three dimensions. We apply periodic quasistatic shear in the same manner as before. For small strains we see that the dynamics settles into a limit cycle (Figs. 13 and 14) similarly to what is observed in two dimensions.

APPENDIX B: CALCULATION OF THE MAXIMAL LYAPUNOV EXPONENT

To establish that a system is chaotic, we have to check whether the system shows sensitivity to initial conditions, which is the main attribute of a chaotic system. Sensitivity to initial conditions means that the distance between different solutions of the equations of motion starting from close-by initial conditions diverges exponentially (see [21] and Fig. 15).

TABLE I. The coefficients in Eq. (A2).

A_0	−1.0
A_1	0.0
A_2	1.785 826 183 464 224
A_3	28.757 894 970 278 530
A_4	−81.988 642 011 620 980
A_5	76.560 294 378 549 440
A_6	−24.115 373 520 671 220

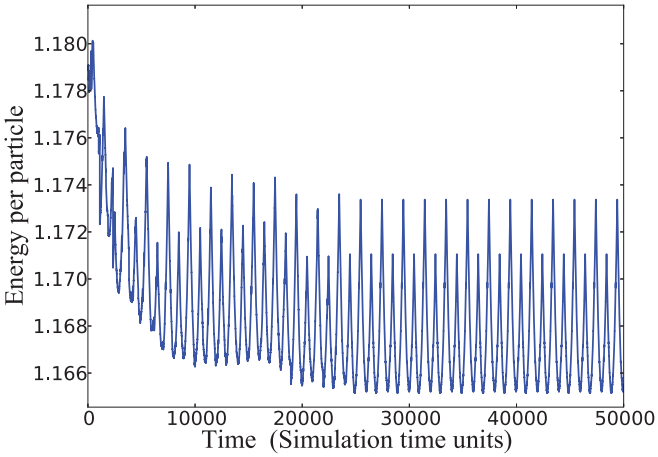

FIG. 13. (Color online) Potential-energy time series for simulations of three-dimensional soft spheres. The maximal strain is $\gamma = 0.05$.

The sensitivity to initial conditions is estimated by measuring the maximal Lyapunov exponent $\lambda_{\max}$ which describes the rate of growth of the distance between two phase-space trajectories (solutions of the equations of motion with different initial conditions), $\mathbf{x}(t)$ and $\mathbf{x}_\epsilon(t)$, which are initially separated by a diminishing distance $|\mathbf{x}(0) - \mathbf{x}_\epsilon(0)| = \epsilon$ [21,22]:

$$\lambda_{\max} = \lim_{t\to\infty} \lim_{\epsilon\to 0} \frac{1}{t} \ln \frac{|\mathbf{x}(t) - \mathbf{x}_\epsilon(t)|}{\epsilon}. \tag{B1}$$

For a periodic system, $\lambda_{\max} = 0$, whereas a chaotic system will have $\lambda_{\max} > 0$ [21]. There are different methods for calculating the maximal Lyapunov exponent. In this work, we used the method suggested by Kantz [22,23], which extracts the largest Lyapunov exponent from a time series of one of the observables (in our case the potential energy: $u_i = \{u_0, u_1, u_2, \ldots\}$). Some of the advantages of this method are that it has been widely tested, a highly tested code is available on the Book web site, and the results provide a relatively clear distinction between chaotic and nonchaotic time series, as we shall see below. Since we are analyzing a time series, instead of looking at the distance between two different solutions of the equations of motion, we look for

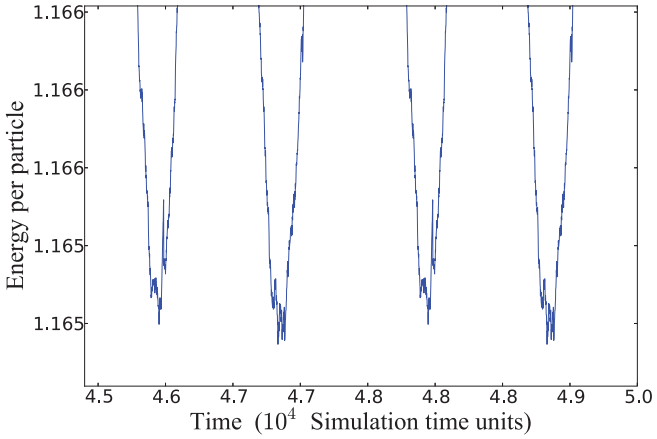

FIG. 14. (Color online) Magnification of the last two cycles in Fig. 13.

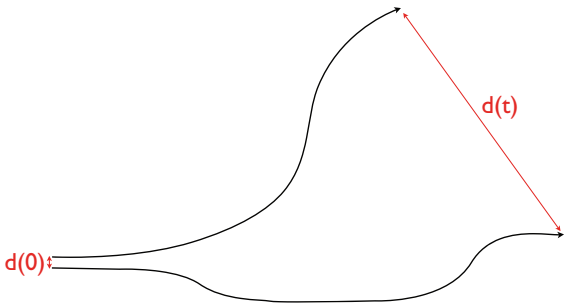

FIG. 15. (Color online) In a chaotic system, the distance between phase-space trajectories diverges exponentially fast.

points in the time series which are at some point close to each other, i.e., $|u_i - u_k| < \epsilon$, and we check how the distance grows over time, $d_\ell = |u_{i+\ell} - u_{k+\ell}|$. However, since u_i is a one-dimensional function of the multidimensional phase space, a simple measure of the distance between them does not reflect the actual distance of the phase-space coordinates that generated them. To overcome this, we use Taken's delay embedding theorem [33], which asserts that for an embedding dimension $m > 2D_A$, where D_A is the dimension of the chaotic attractor (the part in phase space at which the chaotic behavior occurs), a set of m variables generated by sampling the time series at regular intervals τ m,

$$(u_{n-(m-1)\tau}, u_{n-(m-2)\tau}, \ldots, u_{n-\tau}, u_n), \tag{B2}$$

will have an attractor with the same topological properties as the underlying attractor. As an example, we show the reconstruction for the Lorenz system:

$$\begin{aligned} \frac{dx}{dt} &= \sigma(y - x), \quad \frac{dy}{dt} = x(\rho - z) - y, \\ \frac{dz}{dt} &= xy - \beta z. \end{aligned} \tag{B3}$$

In Fig. 16, we show the dynamics as a function of all three coordinates, which shows the famed Lorenz attractor which is chaotic for the parameters that we chose. To demonstrate reconstruction, we take the time series of one of the coordinates

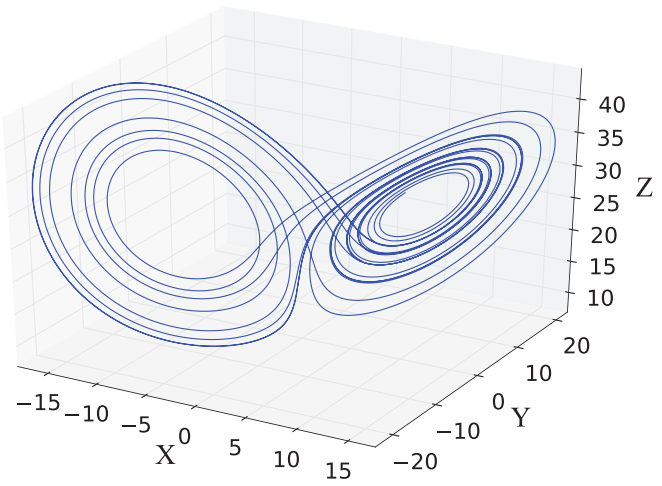

FIG. 16. (Color online) The Lorenz attractor.

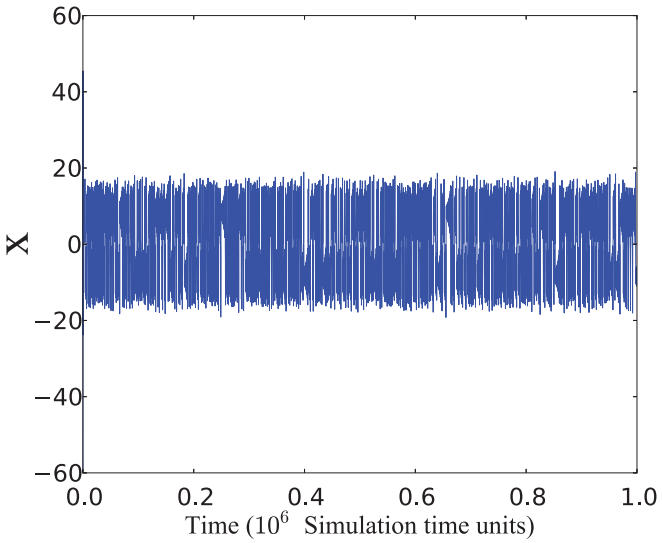

FIG. 17. (Color online) The x coordinate of the Lorenz system.

(Fig. 17) and construct three new coordinates using time delay:

$$(x_{n-2\tau}, x_{n-\tau}, x_n), \tag{B4}$$

where we chose $m = 3$ and an appropriate τ. We now plot the new coordinates in Fig. 18. One can see the resemblance in the structure of the reconstructed attractor and the original one (Fig. 16).

Typically, in a dissipative system, a chaotic attractor will have a smaller dimensionality than the phase-space dimension (in our case the phase-space dimension is $4N$). Defining

$$\mathbf{s}_n = (u_{n-(m-1)\tau}, u_{n-(m-2)\tau}, \ldots, u_{n-\tau}, u_n) \tag{B5}$$

as the delay-coordinates vector, for large enough τ and m, the distance $d = |\mathbf{s}_i - \mathbf{s}_k|$ will represent the actual phase-space distance, and if the underlying dynamics is chaotic, $d_\ell = |\mathbf{s}_{i+\ell} - \mathbf{s}_{k+\ell}|$ will grow exponentially fast. The value of τ is usually taken to be the de-correlation time of the time series ($\tau \approx 600$ in this case), but m is unknown since we do not know *a priori* the dimension of the attractor. To

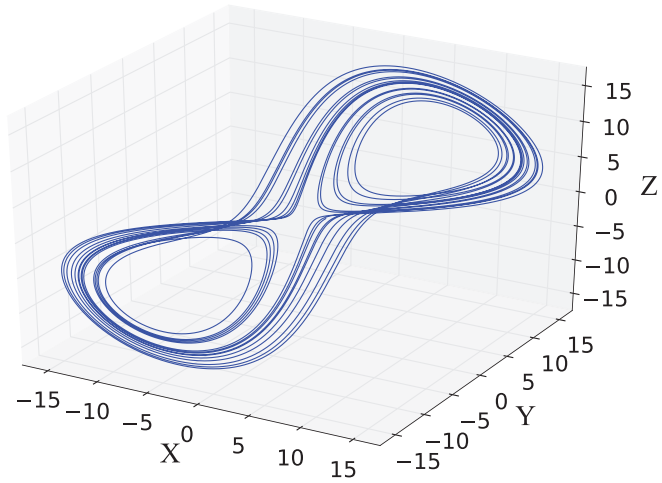

FIG. 18. (Color online) Attractor reconstructed from the x coordinate, which shares the same topological structure as the original attractor.

find a numerical estimate of the largest Lyapunov exponent, the algorithm calculates the finite-time maximal Lyapunov exponent for a trajectory starting at a point i:

$$\lambda_\ell^i = \frac{1}{\ell} \ln \frac{||\mathbf{s}_{i+\ell} - \mathbf{s}_{k+\ell}||}{\epsilon}, \tag{B6}$$

where $||\mathbf{s}_i - \mathbf{s}_k|| < \epsilon$ with respect to some norm $||\cdots||$ (the actual norm used in the algorithm is $||\mathbf{s}_i - \mathbf{s}_k|| = |u_i - u_k|$ for reasons explained in [22]). For each point $\mathbf{s}_i$ and a small distance ϵ, a set of points $\mathbf{s}_k$ such that $||\mathbf{s}_i - \mathbf{s}_k|| < \epsilon$ is gathered, which allows us to calculate the average distance from the point $\mathbf{s}_i$ as a function of ℓ:

$$\lambda_\ell^i = \frac{1}{\ell} \ln \frac{1}{\mathcal{U}_i} \sum_k \frac{||\mathbf{s}_{i+\ell} - \mathbf{s}_{k+\ell}||}{\epsilon}, \tag{B7}$$

where $\mathcal{U}_i$ is the total number of points $\mathbf{s}_k$ that are ϵ close to $\mathbf{s}_i$. The process is repeated for different initial points $\mathbf{s}_i$, which leads to further averaging. The actual function that we calculate is

$$S_\ell = \frac{1}{\mathcal{W}} \sum_i \ln \left(\frac{1}{\mathcal{U}_i} \sum_k \frac{||\mathbf{s}_{i+\ell} - \mathbf{s}_{k+\ell}||}{\epsilon} \right), \tag{B8}$$

where $\mathcal{W}$ is the number of starting points i collected. Since this function describes the ln of the averaged growth of distances as a function of time, we expect that in a chaotic system ($\lambda_{\max} > 0$) S_ℓ will exhibit linear behavior with a positive slope for large enough ℓ. However, there are two caveats for this: the maximal Lyapunov exponent becomes dominant only after several time steps ℓ_0:

$$||\mathbf{s}_{i+\ell} - \mathbf{s}_{k+\ell}|| = \sum_i a_i e^{\lambda_i \ell} \approx_{\ell > \ell_0} a_{\max} e^{\lambda_{\max} \ell}. \tag{B9}$$

The second caveat is that for large ℓ, the distance $||\mathbf{s}_{i+\ell} - \mathbf{s}_{k+\ell}||$ can reach the size of the attractor and thus the trajectories start to fold back. When that happens, S_ℓ saturates. In Fig. 5 we plotted the function S_ℓ for a potential energy time series of a system of size $N = 4096$ sheared at maximal strain amplitudes $\gamma = 0.12$, 0.15, and 0.2, which are all above the critical amplitude. Since the dimension of the attractor is not known *a priori*, we tried all the values of m starting from $m = 1$ until the shape of S_ℓ does not change under further increase (remember that according to Taken's theorem the delay coordinates should give the right result for any $m > 2D_A$, where D_A is the dimension of the attractor). For m values 5, 6, and 6, respectively, the function S_ℓ shows a linear regime with a positive slope, which indicates a positive maximal Lyapunov exponent.

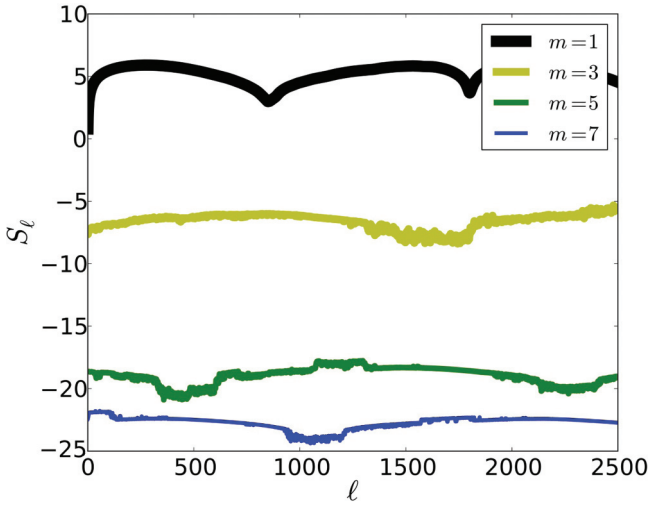

FIG. 19. (Color online) The function S_ℓ applied for a periodic limit cycle. The behavior is strikingly different from that shown in Fig. 5 and includes negative values.

In the main text, we mentioned that the algorithm for calculating the maximal Lyapunov exponent can distinguish between periodic and chaotic behavior. In Fig. 19, we show the result of applying the algorithm for one of the periodic limit cycles with different values of m. One can see that the behavior is significantly different from that observed for the chaotic time series: there is no linear regime and the values of S_ℓ are negative for large enough values of m.

[1] A. S. Argon, Acta Metallurg. **27**, 47 (1979).
[2] C. E. Maloney and A. Lemaître, Phys. Rev. E **74**, 016118 (2006).
[3] P. Schall, D. A. Weitz, and F. Spaepen, Science **318**, 1895 (2007).
[4] M. L. Falk and J. S. Langer, Phys. Rev. E **57**, 7192 (1998).
[5] P. Sollich, Phys. Rev. E **58**, 738 (1998).
[6] P. Sollich, F. Lequeux, P. Hébraud, and M. E. Cates, Phys. Rev. Lett. **78**, 2020 (1997).
[7] L. Bocquet, A. Colin, and A. Ajdari, Phys. Rev. Lett. **103**, 036001 (2009).
[8] N. V. Priezjev, Phys. Rev. E **87**, 052302 (2013).
[9] N. Mangan, C. Reichhardt, and C. J. O. Reichhardt, Phys. Rev. Lett. **100**, 187002 (2008).
[10] L. Corté, P. M. Chaikin, J. P. Gollub, and D. J. Pine, Nat. Phys. **4**, 420 (2008).
[11] D. J. Pine, J. P. Gollub, J. F. Brady, and A. M. Leshansky, Nature (London) **438**, 997 (2005).
[12] S. Slotterback, M. Mailman, K. Ronaszegi, M. van Hecke, M. Girvan, and W. Losert, Phys. Rev. E **85**, 021309 (2012).
[13] G. Petekidis, A. Moussaïd, and P. N. Pusey, Phys. Rev. E **66**, 051402 (2002).
[14] M. Lundberg, K. Krishan, N. Xu, C. S. O'Hern, and M. Dennin, Phys. Rev. E **77**, 041505 (2008).
[15] C. F. Schreck, R. S. Hoy, M. D. Shattuck, and C. S. O'Hern, Phys. Rev. E **88**, 052205 (2013).
[16] N. C. Keim and S. R. Nagel, Phys. Rev. Lett. **107**, 010603 (2011).
[17] N. C. Keim and P. E. Arratia, Soft Matter **9**, 6222 (2013).
[18] E. Bitzek, P. Koskinen, F. Gähler, M. Moseler, and P. Gumbsch, Phys. Rev. Lett. **97**, 170201 (2006).
[19] J. A. Yorke and E. D. Yorke, J. Stat. Phys. **21**, 263 (1979).

[20] T. Tél and Y. C. Lai, Phys. Rep. **460**, 245 (2008).
[21] E. Ott, *Chaos in Dynamical Systems* (Cambridge University Press, Cambridge, 2002).
[22] H. Kantz, Phys. Lett. A **185**, 77 (1994).
[23] H. Kantz and T. Schreiber, *Nonlinear Time Series Analysis*, Vol. 7 (Cambridge University Press, Cambridge, 2004).
[24] Z. Y. Liu, G. Wang, K. C. Chan, J. L. Ren, Y. J. Huang, X. L. Bian, X. H. Xu, D. S. Zhang, Y. L. Gao, and Q. J. Zhai, J. Appl. Phys. **114**, 033521 (2013).
[25] E. J. Banigan, M. K. Illich, D. J. Stace-Naughton, and D. A. Egolf, Nat. Phys. **9**, 288 (2013).
[26] E. Ott and J. C. Sommerer, Phys. Lett. A **188**, 39 (1994).
[27] D. J. Lacks and M. J. Osborne, Phys. Rev. Lett. **93**, 255501 (2004).
[28] E. Bouchbinder, J. S. Langer, and I. Procaccia, Phys. Rev. E **75**, 036108 (2007).
[29] L. Boué, H. G. E. Hentschel, I. Procaccia, I. Regev, and J. Zylberg, Phys. Rev. B **81**, 100201 (2010).
[30] N. C. Keim and P. E. Arratia, arXiv:1308.6806.
[31] D. Fiocco, G. Foffi, and S. Sastry, Phys. Rev. E **88**, 020301(R) (2013).
[32] E. Lerner and I. Procaccia, Phys. Rev. E **79**, 066109 (2009).
[33] F. Takens, *Dynamical Systems and Turbulence, Warwick 1980* (Springer, Berlin, Heidelberg, 1981), pp. 366–381.